FABRICATION OF BIOINSPIRED ARTIFICIAL BACTERIAL FLAGELLA VIA TWO PHOTON LITHOGRAPHY AND WET METALLIZATION

Roberto Bernasconi[1], Gea Prioglio[1], Carlos C. J. Alcantara[2], Salvador Panè[2], and Luca Magagnin[1]*
[1]Dipartimento di Chimica, materiali e Ingegneria Chimica "Giulio Natta",
Politecnico di Milano, Via Mancinelli 7, 20131, Milano (Italy) and
[2]Multi-Scale Robotics Lab, Institute of Robotics and Intelligent Systems,
ETH Zurich, Tannenstrasse 3, CH-8092, Zürich (Switzerland)

2021 21st International Conference on Solid-State Sensors, Actuators and Microsystems (Transducers) | 978-1-6654-1267-4/21/$31.00 ©2021 IEEE | DOI: 10.1109/TRANSDUCERS50396.2021.9495505

ABSTRACT

The present work describes for the first time the production of artificial bacterial flagella (ABFs) by combining laser direct writing and wet metallization. ABFs are helical shaped microrobots that can be remotely actuated using low-strength rotating magnetic fields. They can precisely navigate liquid environments, potentially allowing in-vivo cell and drug delivery or localized microsurgery. ABFs are printed via two photon lithography (2PL) and metallized via electroless deposition. The latter is optimized to yield a nanometric CoNiP layer without damaging the delicate structures. The swimming behavior of the CoNiP coated ABFs is then studied by actuating them inside an array of electromagnetic coils.

KEYWORDS

3D printing, two photon lithography, wet metallization, CoNiP, artificial bacterial flagella.

INTRODUCTION

Bioinspired microrobots are one of the most promising tools for the future of medicine [1]. Thanks to their ability to in-vivo navigate human body, they have been evaluated for a wealth of possible applications: cells [2] and drug [3] delivery, microsurgery [4] and hyperthermia therapy [5]. One of the most explored class of untethered microdevices are artificial bacterial flagella (ABFs). [6] These helical structures, inspired to the flagella of living microorganisms, can be efficiently actuated at the microscale by applying low strength rotating magnetic fields [7]. From the applicative point of view, magnetism constitutes an ideal choice for ABFs actuation due to its non-invasivity towards living tissues and ease of application.

Functionalized ABFs have been proposed for a great number of applications and have been fabricated via a wealth of approaches: templating [8], self-scrolling [9], biopatterning [10] or 3D printing [11]. The latter is of particular importance due to its virtual lack of shape constrains and excellent customizability. The most diffused production route to produce ABFs via 3D printing is the combination of direct laser writing (DLW), the only technique capable of sub-micrometric resolution, with metal evaporation, which is required to impart magnetic properties [12]. In this context, replacing evaporation techniques with alternative metallization technologies, like wet metallization, would result in important advantages. Wet metallization is costless, highly scalable and not susceptible of shadowing effect [13]. Moreover, it allows the deposition of materials characterized by attractive properties like hard magnetic alloys [14] or composites [15].

In the quest of innovative production routes for ABFs, the aim of the present paper is to produce, for the first time, ABFs by combining two photon lithography (2PL, a direct writing technology) with electroless metallization. More in detail, a nanometric CoNiP layer was deposited on 2PL printed devices. Resulting microdevices were characterized from the morphological point of view and actuated inside an array of electromagnetic coils.

The main point of innovation of the present work is the controlled and reproducible wet metallization of microdevices produced via 2PL. More in general, the work demonstrates the possibility to coat micrometric and delicate 3D printed structures with nanometric metallic layers. Another point of innovation present in the work is the use of a semi-hard magnetic alloy on the ABFs, deposited taking advantage of electroless plating. Indeed, most ABFs described in literature are based on the use of soft magnetic materials. The presence of a hard magnetic alloy would potentially result in lower required magnetic field intensity for actuation.

EXPERIMENTAL METHODS

Figure 1 visually depicts the procedure followed for the production of the ABFs. Initially, the devices were printed (figure 1a) using a commercial 2PL setup (Nanoscribe Photonic Professional GT by Nanoscribe GmbH) and the negative photoresist IP-L. A glass slide (170 µm thickness) was used as substrate.

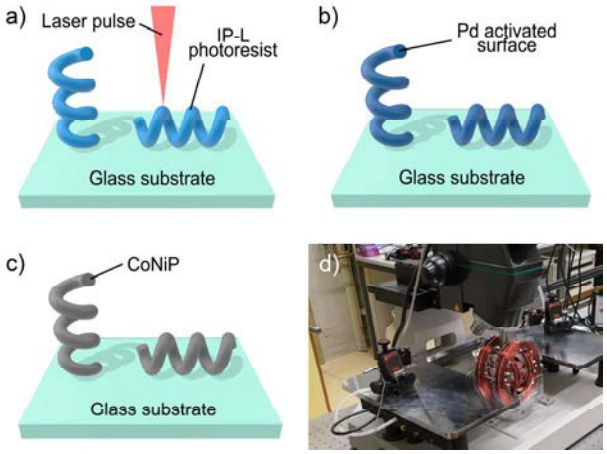

Figure 1: ABFs production scheme and actuation setup.

2PL was carried out using a femtosecond laser with a wavelength of 780 nm. 3-turns helical structures with 5 µm pitch and 5 µm radius were fabricated. Their section was set at 2 µm, while their total length was 15 µm. ABFs were printed vertically on the glass to limit their contact area

with the substrate, minimizing therefore the possible occurrence of imperfections as a result of removal after the metallization process.

At the end of the printing step, ABFs were activated for electroless metallization (figure 1b). A droplet of commercial activator (Neoganth, Atotech) was carefully dispensed on the surface with a pipette and left in contact for 30 s. Then, the droplet was resorbed with the pipette and a second droplet of a reducing solution (20 g/l NaBH4 + 10 g/l NaOH) was dispensed and left in contact for 30 s. Also the second droplet was resorbed with the pipette and the surface was washed in water. By following this procedure, ABFs were activated by the presence of Pd nuclei (figure 1b). Electroless metallization was done immersing the substrate in a room temperature CoNiP electroless solution (figure 1c). Its composition was retrieved from the literature [14]: 0.2 M $NaH_2PO_2 \cdot H_2O$, 0.2 M $(NH_4)_2SO_4$, 0.0163 M $NiSO_4 \cdot 6H_2O$, 0.0087 M $CoSO_4 \cdot 6H_2O$. The base formulation, however, was modified by adding 0.5 ml/l of a 20 % wt. sodium dodecyl sulfate (SDS) solution to improve layer morphology. The glass substrate was immersed horizontally in the electrolyte to avoid the influence of gas bubbles. At the end of the process, substrates were removed from the electrolyte, carefully washed and left to dry in air.

The thickness of the CoNiP plated on the devices was selected keeping in consideration the peculiar actuation methodology employed for ABFs. These devices move under the influence of a rotating magnetic field, which generates a torque according to equation 1.

$$\vec{T} = \int_V \vec{M} \times \vec{B}\, dV = V\, \vec{M} \times \vec{B} \qquad (1)$$

V is the volume of magnetic material, B is the applied external magnetic field and M is the magnetization of the material. It is evident that the torque applied depends on the volume of the magnetic layer, i.e. on its thickness. To ensure sufficient magnetic torque, CoNiP thickness was fixed to 1/10 of the nominal ABFs thickness (100 nm on each side). To obtain this thickness, electroless deposition was carried out for 5 minutes and 20 seconds.

For the actuation tests, single ABFs were manipulated using a microprobe (T-4-22 by GGB Industries Inc.). Samples were carefully transferred from the glass substrate, which was placed inside a sample holder filled with water, to a silicon substrate (placed in the same sample holder). Then, the sample holder was positioned at the center of a Helmholtz setup consisting of three pairs of orthogonal coils (figure 1d). A rotating magnetic field of 1 mT was applied to perform the swimming tests. Videos of the actuation tests were acquired with a microscope and position vs. time data were calculated using Tracker.

RESULTS

At the end of the printing process, and prior to metallization, ABFs were characterized to determine their dimensional adherence to the theoretical measures and to investigate their morphology in view of the metallization step. Figure 2 depicts the SEM appearance of the as printed ABFs.

Figure 2: SEM image of three as printed ABFs.

The first particularity that can be noticed in figure 3 is the presence of some devices that detached from the glass and were found lying horizontally on the substrate. Apparently, they detached during either the printing step or during the subsequent washing to remove uncured resin.

Starting from figure 2, the real dimensions of the ABFs were calculated and compared with the theoretical ones (table 1). The firsts were found to be relatively in line with the latter. The only relevant deviation was recorded on the thickness of the ABFs, which resulted almost 40% higher than the expected one. Thickness, however, depends on the speed of the laser, which determines the cured volume. In this case, a comparatively low laser speed resulted in a thickness in excess.

Table 1: expected vs. experimental dimensions.

Dimension	Experimental (µm)	Theoretical (µm)
Lenght	14.429 ± 0.079	15
Width	5.819 ± 0.029	6
Thickness	2.792 ± 0.027	2
Pitch	4.539 ± 0.137	5

Since the original bath formulation by Homma et al. [14] has been modified adding SDS, the magnetic properties of the CoNiP alloy were determined using Vibrating Sample Magnetometry (VSM). Figure 3 shows the result obtained from a 100 nm CoNiP layer deposited on glass. The out-of-plane magnetic properties of the layer presented in figure 5 are the following: $M_s = 15.88 \cdot 10^{-4}$ emu, $M_r = 1.78 \cdot 10^{-4}$ emu, $H_c = 335$ Oe.

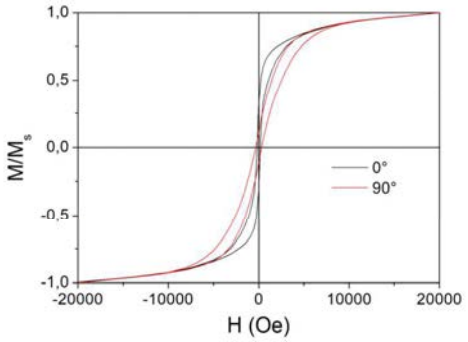

Figure 3: VSM of a 100 nm thick CoNiP layer.

Concerning the in-plane direction, they are: $M_s = 15.98 \cdot 10^{-4}$ emu, $M_r = 4.72 \cdot 10^{-4}$ emu, $H_c = 127$ Oe. The alloy is therefore characterized by a semi-hard magnetic behavior, with magnetic properties slightly lower than the

alloy plated from the SDS-free electrolyte [14].

The magnetic properties observed via VSM can be understood in a better way by investigating the microstructure and the composition of the CoNiP layer. The first was determined by mean of XRD (figure 4).

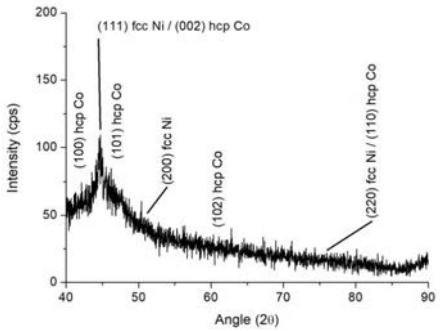

Figure 4: XRD of a 100 nm thick CoNiP layer.

CoNiP presents the peaks typical of hcp Co (JCPDS card no. 05-0727) and fcc Ni (JCPDS card no. 04-0850). These features, however, are relatively broad and not well defined, indicating a lower degree of crystallinity with respect to the SDS-free electrolyte [14]. This particularity reasonably explains the lower magnetic properties observed with the respect to a SDS-free bath.

Chemical composition of the CoNiP was determined via SEM, taking advantage of an EDS module installed on the instrument. The CoNiP had the following composition: 5.98 % P, 26.42 % Co, 67.70 Ni. With respect to the alloy plated form the SDS-free bath [14], Co content is inferior. This is another element that supports the lower magnetic properties observed. SEM was also used to investigate the morphology of the ABFs at the end of the metallization process, as visible in figure 5.

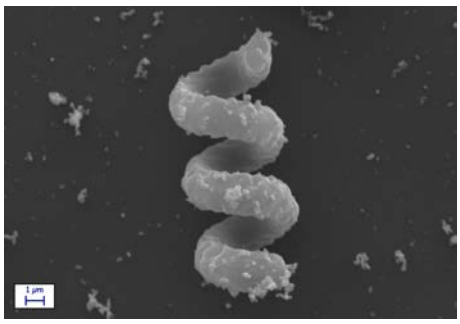

Figure 5: SEM of a CoNiP coated ABF.

As evident, CoNiP uniformly covered the surface of the 3D printed ABFs with a conformal and continuous layer. Most importantly, CoNiP coated also the inner part of the samples, between the spires of the helix. SDS was the key to get such uniformity, as CoNiP plated from SDS-free electrolyte did not plate uniformly on the surface and formed dendrites on the surface of the devices.

CoNiP metallized ABFs were magnetically actuated to verify their controlled motion. As anticipated, a magnetic torque was applied on them. Such torque resulted in a corkscrewing motion [7], in which T can be correlated to the speed of the device considering the relationship expressed by equation 2 [7].

$$\begin{bmatrix} F \\ T \end{bmatrix} = \begin{bmatrix} a & b \\ b & c \end{bmatrix} \begin{bmatrix} v \\ \omega \end{bmatrix} \quad (2)$$

The matrix containing the constants a, b and c is called propulsion matrix. From equation 2, it is evident that the non-fluidic force (F) and torque (T) applied to the ABFs are linearly correlated to their linear (v) and angular (ω) speeds. Moreover, the rotary and translational motions are coupled by the diagonal elements b. Consequently, inducing a rotation on the ABF results into a linear translation. Furthermore, the intensity of such translation is linearly dependent from the rotation frequency of the device, i.e. from the rotation frequency of the external magnetic field B.

When the ABFs are actuated in proximity of a solid surface, however, the forward speed contribution due to corkscrewing (v_{forw}) sums to a lateral drift contribution (v_{drift}), which is dominant. This effect has already been described in literature [16] and is connected to the interaction between the rotating ABF and the substrate. The concept can be clearly visualized by performing a linear actuation (figure 6) and by considering the speed contribution along x (v_{drift}) and y (v_{forw}).

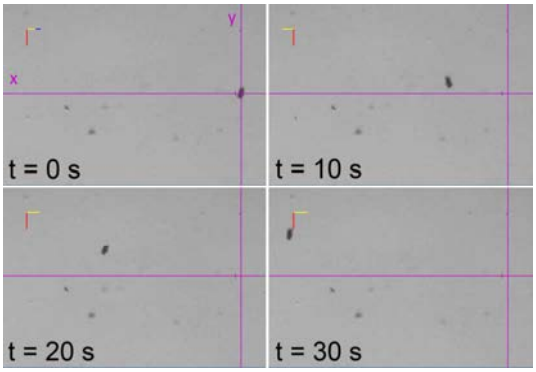

Figure 6: Linear actuation of a CoNiP metallized ABF.

By plotting the position vs. time with respect to the origin of the axis, v_{drift} and v_{forw} can be determined. Figure 7 shows an example recorded at 5 Hz actuation frequency, where v_{forw} is 3.51 µm/s and v_{drift} is 17.94 µm/s.

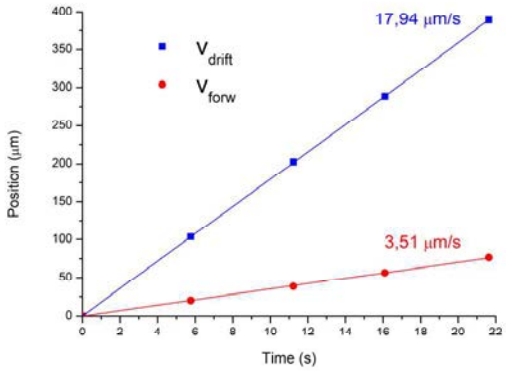

Figure 7: Position vs. time relationship for a single ABF actuated at 5 Hz.

The overall speed of the device (v_{tot}), obtained by the combination of v_{drift} with v_{forw} and measured at different frequencies, follows a linear relationship (figure 8).

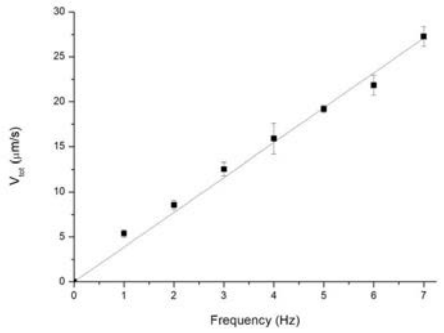

Figure 8: v_{tot} vs. frequency for CoNiP plated ABFs.

By varying the angle of the rotation axis of the magnetic field, ABFs were easily guided along predetermined paths. Figure 9 depicts an example, where the device is actuated along a circular pattern.

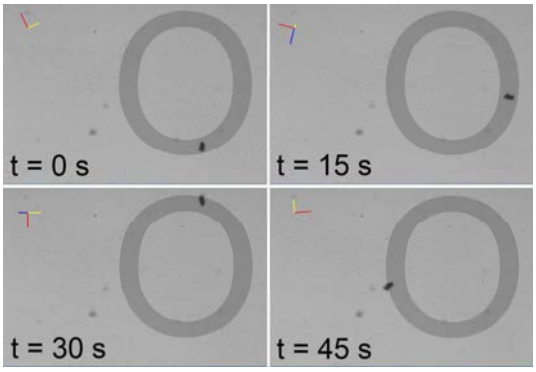

Figure 9: Circular actuation of a single ABF.

As demonstrated in figure 9, CoNiP coated ABFs were characterized by an optimal magnetic controllability.

CONCLUSIONS

Magnetically driven devices were successfully manufactured by combining for the first time laser direct writing and wet metallization. A nanometric layer of CoNiP semi-hard magnetic alloy was deposited on polymeric ABFs with high conformity and good uniformity. The devices were successfully actuated using a low intensity rotating magnetic field, demonstrating a good controllability. The magnetic ABFs described in the present work constitute ideal magnetically navigable platforms that can be further plated with additional metallic layers or surface functionalized to impart specific functionalities. By doing this, for example, tasks like cell or drug delivery and bacteria killing can be carried out.

REFERENCES

[1] S. Palagi, P. Fischer, "Bioinspired microrobots", *Nat. Rev. Mater*, vol. 3, issue 6, pp. 113-124, 2018.

[2] P. Erkoc, I. C. Yasa, H. Ceylan, O. Yasa, Y. Alapan, M. Sitti, "Mobile Microrobots for Active Therapeutic Delivery", *Adv. Ther.*, vol. 2, issue 1, pp. 1800064, 2019.

[3] M. Luo, Y. Feng, T. Wang, J. Guan, "Micro-/Nanorobots at Work in Active Drug Delivery", *Adv. Funct. Mater.*, vol. 28, issue 25, pp. 1706100, 2018.

[4] H. Kim, J. Ali, U. K. Cheang, J. Jeong, J. S. Kim, M. J. Kim, "Micro Manipulation Using Magnetic Microrobots", *J. Bionic Eng.*, vol. 13, issue 4, pp. 515–524, 2016.

[5] J. Park, C. Jin, S. Lee, J.-Y. Kim, H. Choi, "Magnetically Actuated Degradable Microrobots for Actively Controlled Drug Release and Hyperthermia Therapy", *Adv. Healthc. Mater.*, vol. 8, issue16, pp. 1900213, 2019.

[6] L. Zhang, J. J. Abbott, L. Dong, B. E. Kratochvil, D. Bell, B. J. Nelson, "Artificial Bacterial Flagella: Fabrication and Magnetic Control", *Appl. Phys. Lett.*, vol. 94, issue 6, pp. 2007–2010, 2009.

[7] L. Zhang, J. J. Abbott, L. Dong, K. E. Peyer, B. E. Kratochvil, H. Zhang, C. Bergeles, B. J. Nelson, "Characterizing the Swimming Properties of Artificial Bacterial Flagella", *Nano Lett.*, vol. 9, issue 10, pp. 3663–3667, 2009.

[8] M. A. Zeeshan, R. Grisch, E. Pellicer, K. M. Sivaraman, K. E. Peyer, J. Sort, B. Özkale, M. S. Sakar, B. J. Nelson, S. Pané, "Hybrid Helical Magnetic Microrobots Obtained by 3D Template-Assisted Electrodeposition", *Small*, vol. 10, issue 7, pp. 1284-1288, 2014.

[9] L. Zhang, J. J. Abbott, L. Dong, B. E. Kratochvil, D. Bell, B. J. Nelson, "Artificial bacterial flagella: Fabrication and magnetic control", *Appl. Phys. Lett.*, vol. 94, pp. 064107, 2009.

[10] X. Yan, Q. Zhou, M. Vincent, Y. Deng, J. Yu, J. Xu, T. Xu, T. Tang, L. Bian, Y.-X. J. Wang, K. Kostarelos, L. Zhang, "Multifunctional biohybrid magnetite microrobots for imaging-guided therapy", *Sci. Robot.*, vol. 2, pp. eaaq1155, 2017.

[11] J. Ye, D. A. Wilson, Y. Tu, F. Peng, "3D-Printed Micromotors for Biomedical Applications", *Adv. Mater. Tech.*, vol. 5, issue 11, pp. 2000435, 2020.

[12] F. Qiu, R. Mhanna, L. Zhang, Y. Ding, S. Fujita, B. J. Nelson, "Artificial bacterial flagella functionalized with temperature-sensitiveliposomes for controlled release", *Sens. Act. B*, vol. 196, pp. 676–681, 2014.

[13] K. Tansel, "Thin-film growth dynamics with shadowing and re-emission effects", *J. Nanophot.*, vol. 5, issue 1, pp. 052501, 2011.

[14] T. Homma, Y. Sezai, T. Osaka, "A study on growth processes of CoNiP perpendicular magnetic anisotropy films electroless-deposited at room temperature", *Electrochim. Acta*, vol. 42, pp. 3041-3047, 1997.

[15] S.-Y. Liu, J. Ru, F. Liu, "NiP/CuO composites: Electroless plating synthesis, antibiotic photodegradation and antibacterial properties", *Chemosphere*, vol. 267, pp. 129220, 2021.

[16] X. Wang, X.-H. Qin, C. Hu, A. Terzopoulou, X.-Z. Chen, T.-Y. Huang, K. Maniura-Weber, S. Pané, B. J. Nelson, *Adv. Funct. Mater.*, vol. 28, issue 45, pp. 1804107, 2018.

CONTACT

*R. Bernasconi, tel: +39 02 23993150, roberto.bernasconi@polimi.it